

Article

Structure and Mechanical Performance of Poly(vinyl Alcohol) Nanocomposite by Incorporating Graphitic Carbon Nitride Nanosheets

Shaojian He ¹ , Jiaqi Wang ¹, Mengxia Yu ¹, Yang Xue ^{2,*}, Jianbin Hu ¹ and Jun Lin ^{1,*}

¹ Beijing Key Laboratory of Energy Safety and Clean Utilization, North China Electric Power University, Beijing 102206, China; heshaojian@ncepu.edu.cn (S.H.); jqw9542@163.com (J.W.); ymx63162331@163.com (M.Y.); naoh2160@hotmail.com (J.H.)

² State Key Laboratory of Multi-phase Complex Systems, Institute of Process Engineering, Chinese Academy of Sciences, Beijing 100190, China

* Correspondence: xueyang198510@sina.com (Y.X.); jun.lin@ncepu.edu.cn (J.L.); Tel.: +8610-61772185 (J.L.)

Received: 10 March 2019; Accepted: 29 March 2019; Published: 3 April 2019



Abstract: Owing to the high aspect ratio, the two-dimensional (2D) inorganic nanofillers have attracted extensive interest in the field of polymer reinforcement. In this work, graphitic carbon nitride (g-C₃N₄) nanosheets were obtained via thermal condensation of melamine and were then ultrasonically exfoliated in water, which was confirmed by atomic force microscopy (AFM) and TEM. Poly(vinyl alcohol) (PVA)/g-C₃N₄ nanocomposites were achieved by solution casting using water as the solvent. The structure and mechanical performance of PVA/g-C₃N₄ nanocomposites were studied. It was found that the g-C₃N₄ nanosheets were well dispersed in the PVA matrix. The introduction of g-C₃N₄ nanosheets increased the glass transition temperature and crystallinity of the nanocomposites, leading to the improved mechanical performance. Compared with the pure PVA, the PVA/g-C₃N₄ nanocomposite with 0.50 wt% g-C₃N₄ nanosheets showed ~70.7% enhancement in tensile strength, up from 51.2 MPa to 87.4 MPa.

Keywords: poly(vinyl alcohol); graphitic carbon nitride; nanosheets; crystallinity; mechanical performance

1. Introduction

Polymer nanocomposites are among the most important materials in the academic and industrial fields, and are produced by dispersing into the polymeric matrix with nanofillers that have one or more dimensions at nano-scale. Filler dispersion in a polymer matrix is crucial to obtain high-performance nanocomposites [1–3]. Enhancements in the performance of the final nanocomposites depends largely on the morphological aspects of these fillers, such as their sizes and shapes. Among the nanofillers, two-dimensional (2D) nanofillers, including layered silicate, layered double hydroxide (LDH), boron nitride (BN), graphene and graphene oxide (GO), have attracted extensive interest due to the high aspect ratio [4–13]. Compared to the bulk polymers, the polymer nanocomposites filled with 2D nanofillers usually exhibit dramatically different or superior overall performance.

Over the past few years, increasing attention has been paid to graphitic carbon nitride (g-C₃N₄) nanosheets, a promising 2D nanomaterial with a graphene-like structure, which can be synthesized easily, rapidly and inexpensively. The g-C₃N₄ nanosheets have been utilized in many research areas [14–19], which are, however, mostly limited in the field of photocatalysis and heterogeneous catalysis. Recently, Zhu et al. [20] reported that the wear loss of the composite was reduced by introducing g-C₃N₄ as a filler into poly(vinylidene difluoride) (PVDF) matrix. Gang et al. [21] prepared sulfonated poly(ether ether ketone)/g-C₃N₄ nanocomposite membrane with a reduced methanol

permeation. Although $g\text{-C}_3\text{N}_4$ has been used as fillers incorporated into some polymers to improve their performance, the application of $g\text{-C}_3\text{N}_4$ in polymer reinforcement remained rarely explored.

It is expected that the mechanical performance of the polymer can be positively improved by the introduction of $g\text{-C}_3\text{N}_4$ nanosheets, because the structure of $g\text{-C}_3\text{N}_4$ is similar to that of graphene. Moreover, $g\text{-C}_3\text{N}_4$ nanosheets are easily dispersed in water to form stable aqueous suspension due to the weak van der Waals force between the nanosheets [19]. Therefore, in our work, 2D ultrathin $g\text{-C}_3\text{N}_4$ nanosheets were obtained via thermal condensation and were then ultrasonically exfoliated in water, and poly(vinyl alcohol) (PVA)/ $g\text{-C}_3\text{N}_4$ nanocomposites were achieved by environmental-friendly solution blending. The structures of $g\text{-C}_3\text{N}_4$ nanosheets and PVA/ $g\text{-C}_3\text{N}_4$ nanocomposite were analyzed, and the mechanical performance of the nanocomposites were studied to evaluate the effect of using $g\text{-C}_3\text{N}_4$ as the filler for performance improvement of polymer composites.

2. Experimental Section

2.1. Materials

Melamine was purchased from Guangfu Chemical Research Institute, Tianjin, China. PVA (1788) was supplied by Aladdin, Shanghai, China.

2.2. Sample Preparation

Melamine, covered by a tin foil paper in a muffle furnace, was heated to $550\text{ }^\circ\text{C}$ at the heating rate of $10\text{ }^\circ\text{C}/\text{min}$ and maintained at $550\text{ }^\circ\text{C}$ for 2 h. After being cooled in air, the yellow product bulk $g\text{-C}_3\text{N}_4$ was obtained (as illustrated in Figure 1), which was milled into the powder and then dispersed in water with a stirring rate of 13,000 rpm for 30 min. After ultrasonic exfoliation for 48 h, the mixture was left to sit still for 36 h to remove unexfoliated $g\text{-C}_3\text{N}_4$ particles, yielding the stable aqueous suspension of $g\text{-C}_3\text{N}_4$ nanosheets ($\sim 1\text{ mg}/\text{mL}$ in concentration).

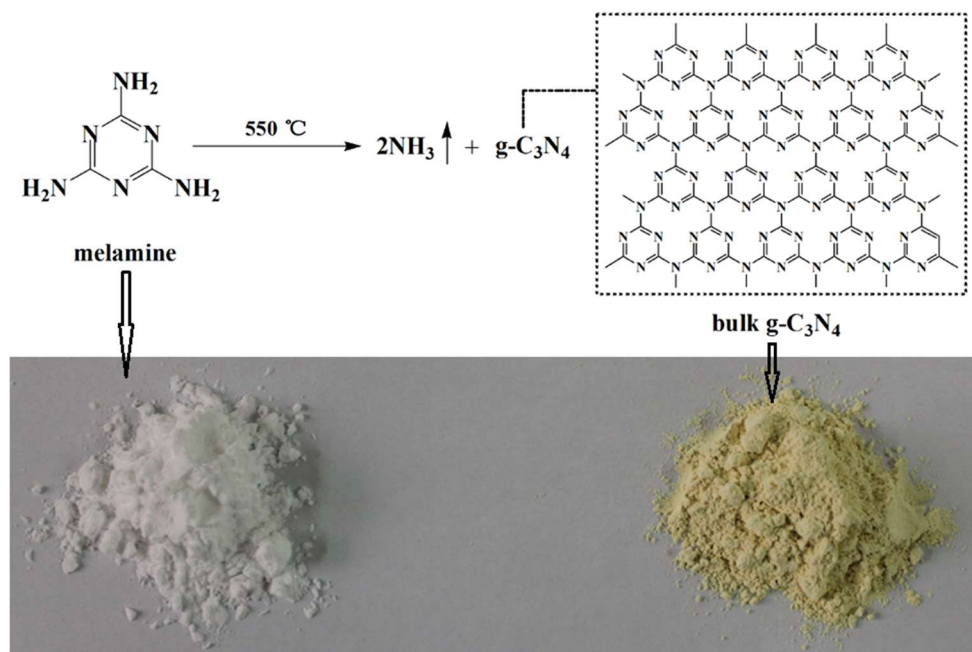


Figure 1. Thermal condensation process from melamine to bulk $g\text{-C}_3\text{N}_4$.

PVA was dissolved in deionized water at $80\text{ }^\circ\text{C}$ for 3 h and then mixed with the aqueous suspension of $g\text{-C}_3\text{N}_4$ nanosheets. The mixture was decanted into a glass dish and dried in an oven at $80\text{ }^\circ\text{C}$ for 36 h, and then dried under vacuum at $60\text{ }^\circ\text{C}$ for 12 h to thoroughly remove the

water. Finally, the prepared film ($\sim 60 \mu\text{m}$ in thickness) was carefully peeled off from the dish to obtain PVA/ $g\text{-C}_3\text{N}_4$ nanocomposite (as illustrated in Figure 2).

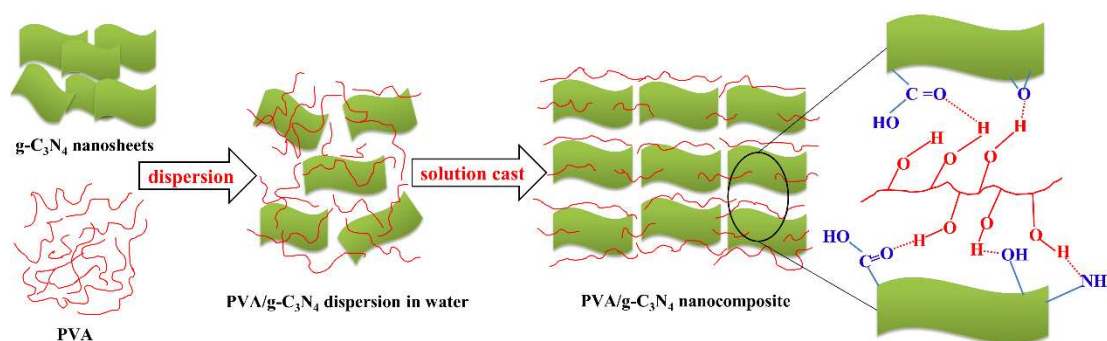


Figure 2. Schematic illustration of nanocomposite preparation and the interaction between $g\text{-C}_3\text{N}_4$ nanosheets and poly(vinyl alcohol (PVA)).

2.3. Measurements

Atomic force microscope (AFM) images were obtained from a SPM-9500 AFM (Shimadzu, Kyoto, Japan) (the dilute dispersions of the samples were drop-cast onto the freshly cleaved silicon surface). Transmission electron microscopy (TEM) images were recorded by a JEM 2010 EX microscope (JEOL, Tokyo, Japan) at an accelerating voltage of 200 kV. Scanning electron microscope (SEM) images were acquired from a JSM-7001F microscope (JEOL) with an acceleration voltage of 20 kV. Differential scanning calorimetry (DSC) experiments were conducted under a nitrogen atmosphere using a STARE system DSC (Mettler-Toledo Co., Schweiz, Switzerland) at a heating rate of $5 \text{ }^\circ\text{C}\cdot\text{min}^{-1}$. The mechanical behavior was characterized according to ISO 527-3-1995 (specimen type 2) using an AI-7000S1 electrical tensile tester (Goodtechwill Testing Machines, Co. Ltd., Qingdao, China) at a speed of $2 \text{ mm}\cdot\text{min}^{-1}$.

3. Results and Discussion

3.1. Characterization of $g\text{-C}_3\text{N}_4$ Nanosheets

The transformation from melamine to $g\text{-C}_3\text{N}_4$ was confirmed by XRD, FTIR and XPS, as shown in the supporting information (Figures S1 and S2). The morphologies of the as-prepared $g\text{-C}_3\text{N}_4$ nanosheets were observed by AFM and TEM. In the AFM images shown in Figure 3, the thickness of the nanosheets is measured to be $2.0\text{--}4.5 \text{ nm}$, indicating that the bulk $g\text{-C}_3\text{N}_4$ was successfully exfoliated into ultrathin nanosheets. Based on the AFM images, the size of the $g\text{-C}_3\text{N}_4$ nanosheets is evaluated to be $50\text{--}80 \text{ nm}$, which is also supported by TEM observation. As shown in Figure 3d,e, the as-prepared $g\text{-C}_3\text{N}_4$ nanosheets consist of stacks of the nanosheets.

3.2. SEM Observation of PVA/ $g\text{-C}_3\text{N}_4$ Nanocomposites

As shown in Figure 4a–c, the similar morphologies are observed for the PVA and PVA/ $g\text{-C}_3\text{N}_4$ nanocomposites with $g\text{-C}_3\text{N}_4$ content of 0.25 wt% and 0.50 wt%, indicating that the $g\text{-C}_3\text{N}_4$ nanosheets are well embedded in the matrix of these two nanocomposites. As illustrated by XPS (Figure S2), there exist $-\text{OH}$, $-\text{NH}_2$ and $-\text{COOH}$ on the surface of $g\text{-C}_3\text{N}_4$ nanosheets, which could form hydrogen bonding with the $-\text{OH}$ groups on PVA macromolecules (as illustrated in Figure 2). As a result, the interfacial interaction would be quite strong in the PVA/ $g\text{-C}_3\text{N}_4$ nanocomposites, leading to the good filler dispersion in the PVA matrix. However, as seen in Figure 4d,e, some $g\text{-C}_3\text{N}_4$ aggregates are exposed on the fractured surface of the nanocomposites, indicating the deteriorated filler dispersion in the matrix when more than 0.50 wt% $g\text{-C}_3\text{N}_4$ nanosheets are added. Moreover, voids are observed in the nanocomposites with $g\text{-C}_3\text{N}_4$ content of 0.75 wt% and 1.00 wt%, demonstrating the severe stress concentration and poor stress transfer in these nanocomposites caused by the filler aggregates.

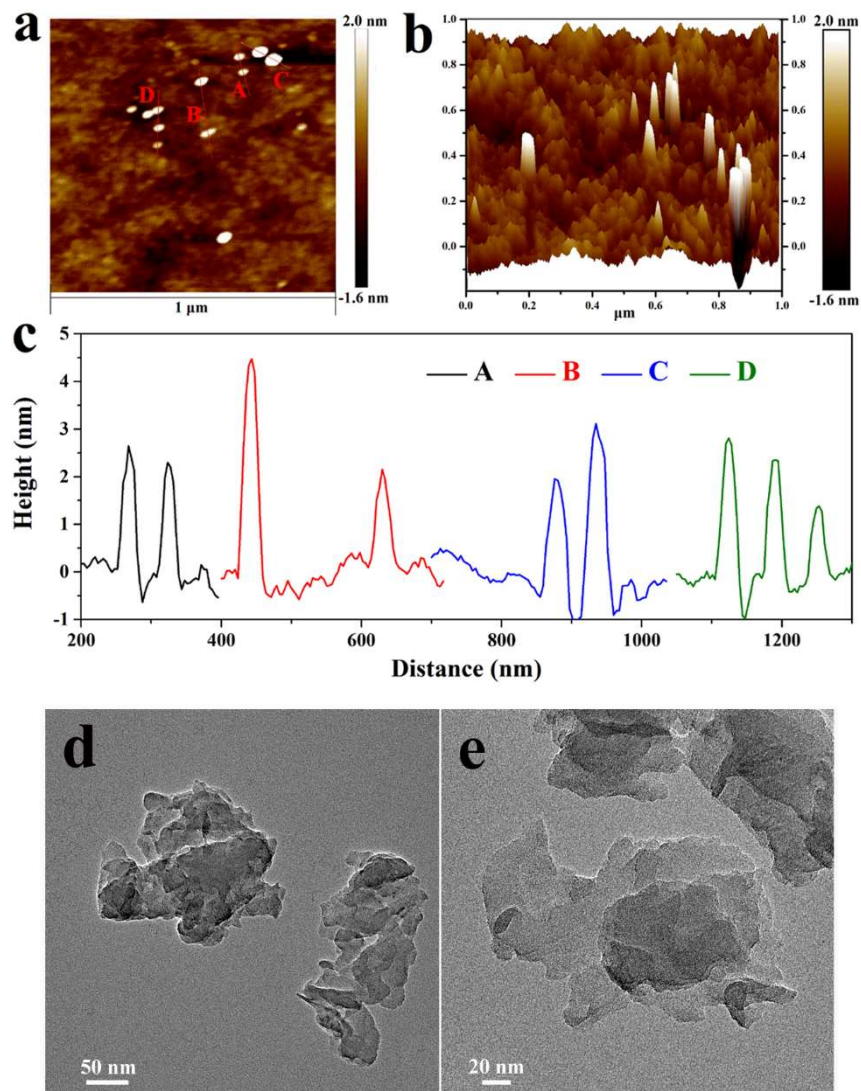


Figure 3. Atomic force microscope (AFM) (a) top view, (b) height topography image, (c) height trace curves of $g\text{-C}_3\text{N}_4$ nanosheets placed on a silicon substrate, and (d,e) TEM images of $g\text{-C}_3\text{N}_4$ nanosheets.

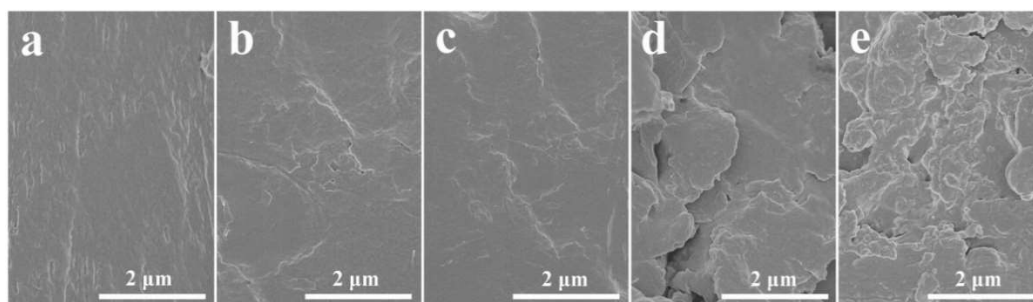


Figure 4. SEM images of tensile fractured surface for (a) pure PVA and PVA/ $g\text{-C}_3\text{N}_4$ nanocomposites with $g\text{-C}_3\text{N}_4$ content of (b) 0.25 wt %, (c) 0.50 wt %, (d) 0.75 wt % and (e) 1.00 wt %.

3.3. XRD of PVA/ $g\text{-C}_3\text{N}_4$ Nanocomposites

XRD curves of $g\text{-C}_3\text{N}_4$ nanosheets, pure PVA and PVA/ $g\text{-C}_3\text{N}_4$ nanocomposites with various $g\text{-C}_3\text{N}_4$ contents are shown in Figure 5. As a typical semi-crystalline polymer, the diffraction peak at 19.5° for the pure PVA should be due to the crystalline phase of the polymer [7]. The XRD patterns

of PVA/g-C₃N₄ nanocomposites with various g-C₃N₄ are similar to that of pure PVA, suggesting that the incorporation of g-C₃N₄ nanosheets into the PVA matrix will not dramatically change the crystal structure of PVA. In addition, the diffraction peaks at 27.7° and 12.8° associated with g-C₃N₄ nanosheets disappear, which should be due to the relatively low content of filler in the nanocomposites.

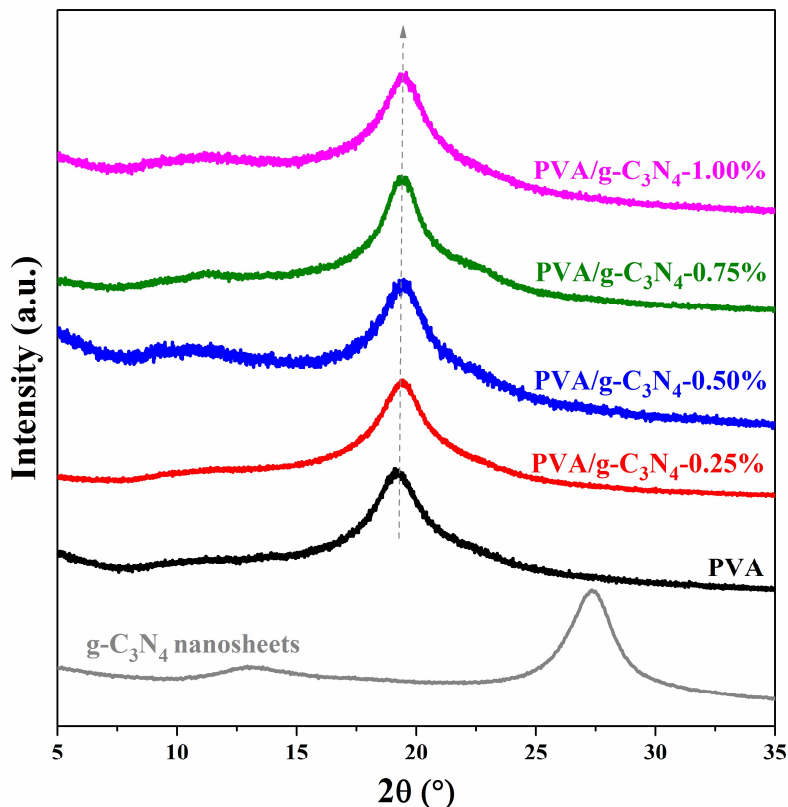


Figure 5. XRD curves of PVA/g-C₃N₄ nanocomposites with various g-C₃N₄ contents.

3.4. DSC Analysis of PVA/g-C₃N₄ Nanocomposites

The glass transition temperature (T_g), melting temperature (T_m) and melting enthalpy (ΔH_m) of the pure PVA and PVA/g-C₃N₄ nanocomposites were obtained from the DSC curves, as shown in Figure 6. It was found that the T_g s of the PVA/g-C₃N₄ nanocomposites were all higher than that of pure PVA and increased with the increasing g-C₃N₄ content. By adding only 1.00 wt% g-C₃N₄, the T_g significantly increased from 57.2 °C for pure PVA to 65.5 °C for the nanocomposite. Such an increase should be ascribed to the strong mobility restriction of PVA chain segments by the g-C₃N₄ nanosheets. Moreover, as shown in Figure 6, there exhibits little difference for the T_m between the pure PVA and PVA/g-C₃N₄ nanocomposites. By taking 138.6 J/g as the melting enthalpy for the perfect crystalline PVA [22], the calculated crystallinities of the nanocomposites are illustrated in Figure 6. With the increase of g-C₃N₄ content, the crystallinity of PVA/g-C₃N₄ nanocomposites first increases until reaching a maximum of 25.9% at 0.50 wt% g-C₃N₄ content and then dropped to 22.2% at 1.00 wt% g-C₃N₄ content, still higher than that of pure PVA (20.5%). Such results may be rationalized as follows: the increased crystallinity for the composites with a relatively low content of nanoparticles is often observed, as widely reported in the literature [23–25], because the small number of nanoparticles, serving as nucleating agents, could promote polymer crystallization. However, when more g-C₃N₄ is incorporated, these nanosheets might gather to form aggregates and weaken their promotion effect on the PVA crystallization, leading to a slight decline in crystallinity. Therefore, the crystallinity of PVA/g-C₃N₄ nanocomposites first rises and then declines with the increasing g-C₃N₄ content.

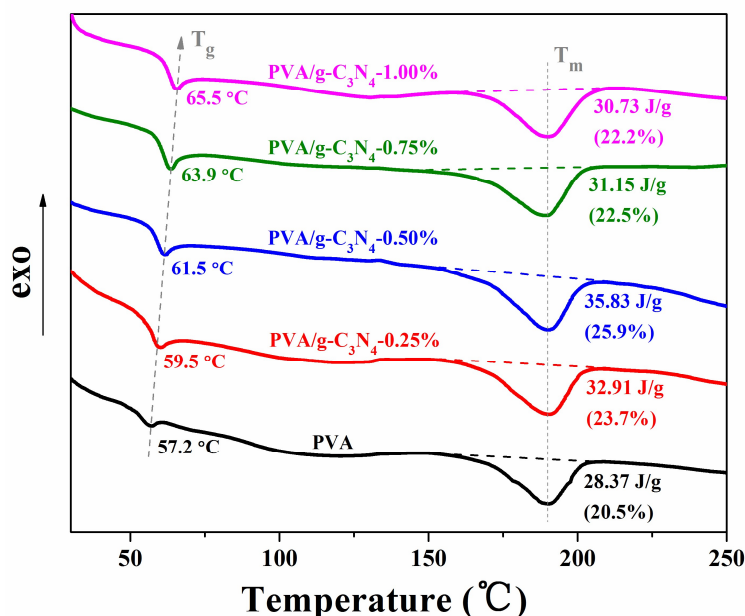


Figure 6. DSC curves of pure PVA and PVA/g-C₃N₄ nanocomposites.

3.5. Mechanical Performance of PVA/g-C₃N₄ Nanocomposites

The mechanical performance for pure PVA and PVA/g-C₃N₄ nanocomposites is presented in Table 1, and the stress–strain curves for these nanocomposites are shown in Figure 7. Compared to those of the pure PVA, the elastic modulus, yield strength and tensile strength of the PVA/g-C₃N₄ nanocomposite with g-C₃N₄ content of 0.5 wt% increase by ~66.7%, ~69.5% and ~70.7%, respectively, while the elongation at break declines by ~8.9%. With further increasing g-C₃N₄ content to 1.00 wt%, the elastic modulus, yield strength and tensile strength slightly decrease, but still higher than those of pure PVA. Usually, higher crystallinity corresponds to the higher elastic modulus and strength. Therefore, the change of mechanical performance of PVA/g-C₃N₄ nanocomposites is similar to that of the crystallinity as a function of the g-C₃N₄ content. The PVA/g-C₃N₄ nanocomposite containing 0.50 wt% g-C₃N₄ has the highest crystallinity, leading to the strongest elastic modulus and strength. When the applied strain beyond the yield strain, the irreversible forced high-elastic deformation takes place, which originates from the forced motion of the polymeric chain segments under stress. For PVA/g-C₃N₄ nanocomposites, such motion may be restricted by the presence of g-C₃N₄ nanosheets. In addition, the good dispersion of g-C₃N₄ nanosheets in the nanocomposites with a relatively low content from 0.25 wt% to 0.50 wt% also results in the good stress transfer, facilitating the excellent reinforcement. Moreover, as shown in Table 2, ~70.7% improvement of the tensile strength in our work is comparable with or even higher than those of the PVA nanocomposites filled with various 2D nanofillers in the previous reports. Therefore, the g-C₃N₄ nanosheets exhibit an exciting potential as the filler for the reinforcement of polymeric materials.

Table 1. Mechanical performance of pure PVA and PVA/g-C₃N₄ nanocomposites.

Content of g-C ₃ N ₄ (wt %)	0	0.25	0.50	0.75	1.00
Elastic modulus (GPa)	2.28 ± 0.12	3.66 ± 0.17	3.80 ± 0.14	2.62 ± 0.09	2.48 ± 0.08
Yield strength (MPa)	55.1 ± 1.7	75.6 ± 2.1	93.4 ± 3.8	69.4 ± 1.9	63.6 ± 2.2
Tensile strength (MPa)	51.2 ± 2.8	82.3 ± 3.2	87.4 ± 2.6	74.3 ± 1.9	66.8 ± 2.3
Elongation at break (%)	124 ± 8	123 ± 7	113 ± 5	143 ± 11	129 ± 7

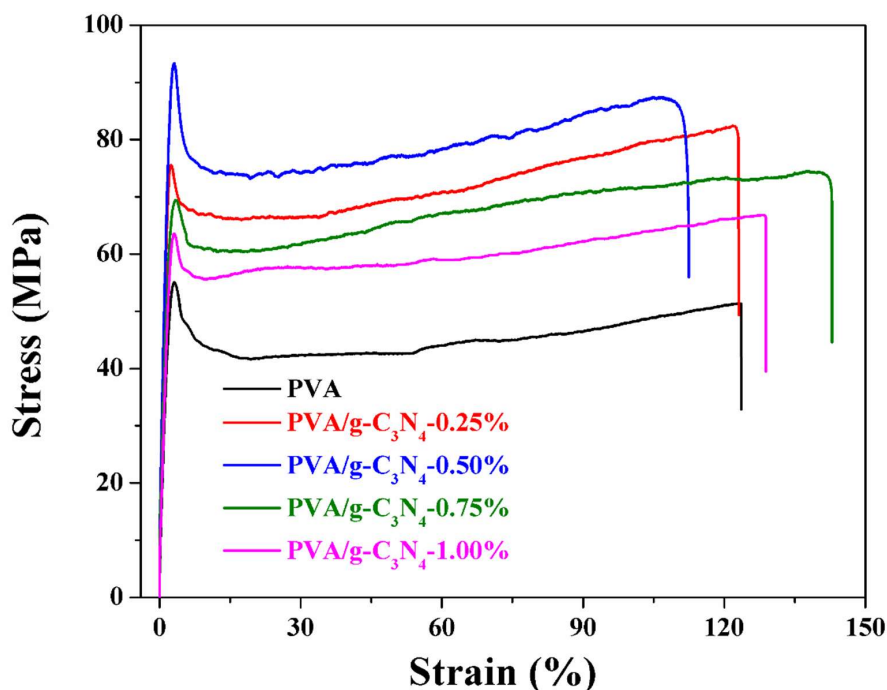


Figure 7. Stress–strain curves of pure PVA and PVA/g-C₃N₄ nanocomposites.

Table 2. Comparison of the improvement in tensile strength for the PVA nanocomposites filled with 2D nanofillers.

Filler	Content (wt%)	Tensile strength (MPa)		Improvement (%)	Reference
		Pure PVA	Nanocomposite		
graphene ^a	3.0	17.0	42.0	~147	[26]
	0.5		27.0	~58.8	
graphene ^b	1.8	33.5	113	~237	[7]
	0.7		67.6	~101	
GO	0.3		65.0	~94.0	[6]
	2.0	22.5	45.7	~103	
	0.5		32.1	~42.7	
BN	0.8	77.0	91.0	~18.2	[27]
BN	2.0	46.0	99.2	~115	[28]
	0.5		81.5	~77.1	
LDH	1.0	58.9	114	~93.0	[8]
	0.5		88.1	~49.6	
LDH ^b	2.0	28.3	47.0	~66.0	[29]
MoS ₂	5.0	84.0	105	~24.0	[30]
montmorillonite	1.0	~62.0	~68.5	~10.5	[31]
g-C ₃ N ₄	0.5	51.2	87.4	~70.7	Our work

^a The mass fraction was converted from the volume fraction according to the related density mentioned in the reference; ^b the filler was modified by the organic component.

4. Conclusions

In this work, an attempt has been made to evaluate the effect of using g-C₃N₄ nanosheets on the mechanical performance of polymer composites. After thermal condensation of melamine, the as-prepared bulk g-C₃N₄ were ultrasonically exfoliated in water to form a stable aqueous suspension of g-C₃N₄ nanosheets. The successful exfoliation of g-C₃N₄ nanosheets was observed by AFM and TEM. The mixture of aqueous PVA solution and g-C₃N₄ nanosheets suspension was cast to prepare the PVA/g-C₃N₄ nanocomposites. As demonstrated by SEM, the g-C₃N₄ nanosheets were well dispersed in the PVA matrix. Moreover, by introducing g-C₃N₄ nanosheets in the PVA matrix, the

nanocomposites exhibited the higher glass transition temperature and crystallinity as compared to the pure PVA, resulting in the improved mechanical performance. Therefore, the present study demonstrates that the g-C₃N₄ nanosheets could be applied as a promising filler to effectively reinforce polymer to achieve high-performance.

Supplementary Materials: The following are available online at <http://www.mdpi.com/2073-4360/11/4/610/s1>, Figure S1: (a) XRD and (b) FTIR curves of melamine, bulk g-C₃N₄ and g-C₃N₄ nanosheets; Figure S2: XPS (a) survey scan, (b) N1s, (c) C1s and (d) O1s of g-C₃N₄ nanosheets.

Author Contributions: Data curation, S.H., J.W., M.Y. and J.H.; formal analysis, S.H. and Y.X.; funding acquisition, J.L.; investigation, S.H.; methodology, J.W.; supervision, Y.X. and J.L.; writing—original draft, S.H.; writing—review and editing, Y.X. and J.L..

Funding: This work was supported by the National Natural Science Foundation of China, China (51773058), and the National Engineering Laboratory for Ultra High Voltage Engineering Technology (Kunming, Guangzhou), China (NEL201808), and the Fundamental Research Funds for the Central Universities, China (2016YQ08). The APC was funded by the National Natural Science Foundation of China, (51773058).

Conflicts of Interest: The authors declare no conflict of interest.

References

1. Ma, P.C.; Siddiqui, N.A.; Marom, G.; Kim, J.K. Dispersion and functionalization of carbon nanotubes for polymer-based nanocomposites: A review. *Compos. Part A* **2010**, *41*, 1345–1367. [[CrossRef](#)]
2. He, S.J.; Hu, J.B.; Zhang, C.; Wang, J.Q.; Chen, L.; Bian, X.M.; Lin, J.; Du, X.Z. Performance improvement in nano-alumina filled silicone rubber composites by using vinyl tri-methoxysilane. *Polym. Test.* **2018**, *67*, 295–301. [[CrossRef](#)]
3. Liu, M.; Jia, Z.; Jia, D.; Zhou, C. Recent advance in research on halloysite nanotubes-polymer nanocomposite. *Prog. Polym. Sci.* **2014**, *39*, 1498–1525. [[CrossRef](#)]
4. He, S.J.; Bai, F.J.; Liu, S.X.; Ma, H.F.; Hu, J.B.; Chen, L.; Lin, J.; Wei, G.S.; Du, X.Z. Aging properties of styrene-butadiene rubber nanocomposites filled with carbon black and rectorite. *Polym. Test.* **2017**, *64*, 92–100. [[CrossRef](#)]
5. Xue, Y.; Li, X.F.; Wang, H.S.; Zhang, D.H.; Chen, Y.F. Thermal conductivity improvement in electrically insulating silicone rubber composites by the construction of hybrid three-dimensional filler networks with boron nitride and carbon nanotubes. *J. Appl. Polym. Sci.* **2019**, *136*, 46929. [[CrossRef](#)]
6. Cheng, H.K.F.; Sahoo, N.G.; Tan, Y.P.; Pan, Y.; Bao, H.; Li, L.; Chan, S.H.; Zhao, J. Poly(vinyl alcohol) Nanocomposites Filled with Poly(vinyl alcohol)-Grafted Graphene Oxide. *ACS Appl. Mater. Inter.* **2012**, *4*, 2387–2394. [[CrossRef](#)]
7. Tang, Z.; Lei, Y.; Guo, B.; Zhang, L.; Jia, D. The use of rhodamine B-decorated graphene as a reinforcement in polyvinyl alcohol composites. *Polymer* **2012**, *53*, 673–680. [[CrossRef](#)]
8. Du, M.; Ye, W.; Lv, W.; Fu, H.; Zheng, Q. Fabrication of high-performance poly(vinyl alcohol)/MgAl-layered double hydroxide nanocomposites. *Eur. Polym. J.* **2014**, *61*, 300–308. [[CrossRef](#)]
9. Park, G.T.; Chang, J.H. Comparison of Properties of PVA Nanocomposites Containing Reduced Graphene Oxide and Functionalized Graphene. *Polymers* **2019**, *11*, 450. [[CrossRef](#)]
10. Sanchez-Hidalgo, R.; Blanco, C.; Menendez, R.; Verdejo, R.; Lopez-Manchado, M.A. Multifunctional Silicone Rubber Nanocomposites by Controlling the Structure and Morphology of Graphene Material. *Polymers* **2019**, *11*, 449. [[CrossRef](#)]
11. He, S.J.; He, T.F.; Wang, J.Q.; Wu, X.H.; Xue, Y.; Zhang, L.Q.; Lin, J. A novel method to prepare acrylonitrile-butadiene rubber/clay nanocomposites by compounding with clay gel. *Compos. Part B* **2019**, *167*, 356–361. [[CrossRef](#)]
12. Wang, X.; Liu, X.; Yuan, H.; Liu, H.; Liu, C.; Li, T.; Yan, C.; Yan, X.; Shen, C.; Guo, Z. Non-covalently functionalized graphene strengthened poly(vinyl alcohol). *Mater. Design* **2018**, *139*, 372–379. [[CrossRef](#)]
13. Shi, X.; Yang, P.; Peng, X.; Huang, C.; Qian, Q.; Wang, B.; He, J.; Liu, X.; Li, Y.; Kuang, T. Bi-phase fire-resistant polyethylenimine/graphene oxide/melanin coatings using layer by layer assembly technique: Smoke suppression and thermal stability of flexible polyurethane foams. *Polymer* **2019**, *170*, 65–75. [[CrossRef](#)]
14. Zhao, Z.; Sun, Y.; Dong, F. Graphitic carbon nitride based nanocomposites: a review. *Nanoscale* **2015**, *7*, 15–37. [[CrossRef](#)]

15. Su, F.; Mathew, S.C.; Lipner, G.; Fu, X.; Antonietti, M.; Blechert, S.; Wang, X. mpg-C₃N₄-Catalyzed Selective Oxidation of Alcohols Using O₂ and Visible Light. *J. Am. Chem. Soc.* **2010**, *132*, 16299–16301. [[CrossRef](#)]
16. Wang, Z.; Guan, W.; Sun, Y.; Dong, F.; Zhou, Y.; Ho, W.K. Water-assisted production of honeycomb-like g-CN with ultralong carrier lifetime and outstanding photocatalytic activity. *Nanoscale* **2015**, *7*, 2471–2479. [[CrossRef](#)]
17. Yang, S.; Gong, Y.; Zhang, J.; Zhan, L.; Ma, L.; Fang, Z.; Vajtai, R.; Wang, X.; Ajayan, P.M. Exfoliated Graphitic Carbon Nitride Nanosheets as Efficient Catalysts for Hydrogen Evolution Under Visible Light. *Adv. Mater.* **2013**, *25*, 2452–2456. [[CrossRef](#)] [[PubMed](#)]
18. Ding, X.; Zhu, J.; Yue, Z.; Qian, X.; Bi, W.; Yang, X.; Yang, J. Separation and concentration of natural products by fast forced adsorption using well-dispersed velvet-like graphitic carbon nitride with response surface methodology optimisation. *Talanta* **2016**, *154*, 119–126. [[CrossRef](#)] [[PubMed](#)]
19. Dong, G.; Zhang, Y.; Pan, Q.; Qiu, J. A fantastic graphitic carbon nitride (g-C₃N₄) material: Electronic structure, photocatalytic and photoelectronic properties. *J. Photoch. Photobio. C* **2014**, *20*, 33–50. [[CrossRef](#)]
20. Zhu, L.; Wang, Y.; Hu, F.; Song, H.J. Structural and friction characteristics of g-C₃N₄/PVDF composites. *Appl. Surf. Sci.* **2015**, *345*, 349–354. [[CrossRef](#)]
21. Gang, M.; He, G.; Li, Z.; Cao, K.; Li, Z.; Yin, Y.; Wu, H.; Jiang, Z. Graphitic carbon nitride nanosheets/sulfonated poly(ether ether ketone) nanocomposite membrane for direct methanol fuel cell application. *J. Membr. Sci.* **2016**, *507*, 1–11. [[CrossRef](#)]
22. Peppas, N.A.; Merrill, E.W. Differential scanning calorimetry of crystallized PVA hydrogels. *J. Appl. Polym. Sci.* **1976**, *20*, 1457–1465. [[CrossRef](#)]
23. Ning, N.Y.; Fu, S.R.; Zhang, W.; Chen, F.; Wang, K.; Deng, H.; Zhang, Q.; Fu, Q. Realizing the enhancement of interfacial interaction in semicrystalline polymer/filler composites via interfacial crystallization. *Prog. Polym. Sci.* **2012**, *37*, 1425–1455. [[CrossRef](#)]
24. Xu, J.Z.; Zhong, G.J.; Hsiao, B.S.; Fu, Q.; Li, Z.M. Low-dimensional carbonaceous nanofiller induced polymer crystallization. *Prog. Polym. Sci.* **2014**, *39*, 555–593. [[CrossRef](#)]
25. Shi, S.; Wang, L.; Pan, Y.; Liu, C.; Liu, X.; Li, Y.; Zhang, J.; Zheng, G.; Guo, Z. Remarkably Strengthened microinjection molded linear low-density polyethylene (LLDPE) via multi-walled carbon nanotubes derived nanohybrid shish-kebab structure. *Compos. Part B* **2019**, *167*, 362–369. [[CrossRef](#)]
26. Zhao, X.; Zhang, Q.; Chen, D.; Lu, P. Enhanced Mechanical Properties of Graphene-Based Poly(vinyl alcohol) Composites. *Macromolecules* **2010**, *43*, 2357–2363. [[CrossRef](#)]
27. Zhang, J.; Lei, W.; Liu, D.; Wang, X. Synergistic influence from the hybridization of boron nitride and graphene oxide nanosheets on the thermal conductivity and mechanical properties of polymer nanocomposites. *Compos. Sci. Technol.* **2017**, *151*, 252–257. [[CrossRef](#)]
28. Duan, Z.Q.; Liu, Y.T.; Xie, X.M.; Ye, X.Y. A simple and green route to transparent boron nitride/PVA nanocomposites with significantly improved mechanical and thermal properties. *Chin. Chem. Lett.* **2013**, *24*, 17–19. [[CrossRef](#)]
29. Xie, J.; Zhang, K.; Wang, Z.; Zhao, Q.; Yang, Y.; Zhang, Y.; Ai, S.; Xu, J. Biodegradable poly(vinyl alcohol)-based nanocomposite film reinforced with organophilic layered double hydroxides with potential packaging application. *Iran. Polym. J.* **2017**, *26*, 811–819. [[CrossRef](#)]
30. Zhou, K.; Jiang, S.; Bao, C.; Song, L.; Wang, B.; Tang, G.; Hu, Y.; Gui, Z. Preparation of poly(vinyl alcohol) nanocomposites with molybdenum disulfide (MoS₂): Structural characteristics and markedly enhanced properties. *RSC Adv.* **2012**, *2*, 11695–11703. [[CrossRef](#)]
31. Li, C.; Li, Y.; She, X.; Vongsvivut, J.; Li, J.; She, F.; Gao, W.; Kong, L. Reinforcement and deformation behaviors of polyvinyl alcohol/graphene/montmorillonite clay composites. *Compos. Sci. Technol.* **2015**, *118*, 1–8. [[CrossRef](#)]

